EPJ E
Soft Matter and Biological Physics
EPJ.org
your physics journal

Eur. Phys. J. E (2012) **35**: 79 DOI 10.1140/epje/i2012-12079-8

Role of metal ions in growth and stability of Langmuir-Blodgett films on homogeneous and heterogeneous surfaces

J.K. Bal, Sarathi Kundu and S. Hazra

edp sciences Società Italiana di Fisica Springer

Eur. Phys. J. E (2012) **35**: 79
DOI 10.1140/epje/i2012-12079-8

THE EUROPEAN PHYSICAL JOURNAL E

Regular Article

Role of metal ions in growth and stability of Langmuir-Blodgett films on homogeneous and heterogeneous surfaces

J.K. Bal[1,a], Sarathi Kundu[2], and S. Hazra[1]

[1] Surface Physics Division, Saha Institute of Nuclear Physics, 1/AF Bidhannagar, Kolkata 700064, India
[2] Physical Sciences Division, Institute of Advanced Study in Science and Technology, Vigyan Path, Paschim Boragaon, Garchuk, Guwahati, Assam 781035, India

Received 3 March 2012 and Received in final form 27 May 2012
Published online: 24 August 2012 –

Abstract. Structure and stability of cadmium arachidate (CdA) Langmuir-Blodgett (LB) films on homogeneous (*i.e.*, OH-, H-passivated Si(001) substrates) and heterogeneous (*i.e.*, Br-passivated Si(001) substrates) surfaces were studied using X-ray reflectivity and atomic force microscopy techniques and compared with those of nickel arachidate (NiA) LB films. While on OH-passivated Si, an asymmetric monolayer (AML) structure starts to grow, on H-passivated Si, a symmetric monolayer (SML) of CdA forms, although for both the films, pinhole-type defects are present as usual. However, on heterogeneous Br-passivated Si substrates, a combination of AML, SML, shifted SML and SML on top of AML (*i.e.*, AML/SML), all types of structures are found to grow in such a way that, due to the variation of heights in the out-of-plane direction, ring-shaped in-plane nanopatterns of CdA molecules are generated. Probably due to stronger head-head interactions and higher metal ion-carboxylic ligand bond strength for CdA molecules compared to NiA, easy flipping of SML on top of another preformed SML, *i.e.* a SML/SML structure formation was not possible and as a result a wave-like modulation is observed for the CdA film on such heterogeneous substrate. The presence of hydrophilic/hydrophobic interfacial stress on the heterogeneous substrate thus modifies the deposited molecular structure so that the top surface morphology for a CdA film is similar to monolayer buckling while that for NiA film is similar to monolayer collapse.

1 Introduction

Amphiphiles having hydrophilic heads and hydrophobic tails are interesting molecules, as they form order Langmuir monolayers at the air-water interface [1]. The ordering of such Langmuir monolayer, in general, improves through metal ions-carboxylic headgroups interaction, when metal ions are present in subphase water [2,3]. However, the amount of improvement depends upon the nature of interaction, *i.e.* the nature of metal ions. For example, the interaction is found to be higher for the divalent metals having covalent nature compared to those having ionic nature and accordingly, different ordered or structured Langmuir monolayers are observed [4–6]. Langmuir monolayers containing metal ions can be easily transferred to solid substrates to form ordered metal-organic multilayered Langmuir-Blodgett (LB) films [2,7,8]. Such LB films are ideal for testing physics of low-dimensional systems and have promising applications in the field of biosensor, catalysis and nanotechnology [2,9–13]. However, most of the proposed applications, arising from the unique physical properties of LB films, strongly depend on their structure, and hence control of the specific structure through proper understanding is important.

The structure of a LB film is strongly related to two main factors: the structure or order of the starting Langmuir monolayer and the substrate-surface condition where it is transferred. The structure of the Langmuir monolayer can be tuned through selection of different metal ions, having different type and/or strength of interaction, as mentioned before [4,6]. This can give rise to different structured LB films [14,15]. Similarly, it has been observed that the increase in *p*H helps to incorporate more metal ions in the monolayer and thereby decreases the pinhole-like defects in the LB films [16]; also the increase in surface pressure beyond standard monolayer formation, either buckles [17–19] and/or collapses [20–25] the Langmuir monolayer and shows different structured film, when transferred to solid substrate.

The polar-nonpolar (*i.e.* hydrophilic-hydrophobic) nature of a substrate-surface, arising from the passivation or termination of a surface with a foreign atomic layer (such as hydrogen, bromine, etc.) [26–31], changes the initial attachment of the monolayer, which leads to different structured LB films. For example, nickel arachidate (NiA) LB films show an asymmetric monolayer (AML) structure

[a] e-mail: jayanta.bal@gmail.com

on an OH-terminated surface and a symmetric monolayer (SML) structure on H-terminated surface, consistent with the hydrophilic and hydrophobic nature of the substrates, respectively, while they show both AML and SML structures on Br-terminated surface *i.e.*, AML+SML structure, suggesting a coexisting (hydrophilic and hydrophobic) nature of the substrate. Although the *p*H of the subphase water (~ 9) is high, the SML structure that is formed on H-terminated surface is found quite disordered and unstable, while the Br-terminated surface shows an unusual growth behavior, namely hydrophilic and hydrophobic attachments of NiA molecules in single up stroke of deposition and growth of large heights of ring-shaped islands in subsequent deposition. The latter arises due to flipping of molecules to release the initially accumulated stress in the film structures near hydrophilic/hydrophobic interface, which is similar to the collapse of monolayer due to application of pressure.

Now the question is if we replace Ni ions, which interact electrostatically (*i.e.* less strongly) with the arachidic acid headgroups to form NiA Langmuir monolayer [32], with, say, Cd ions, which interact covalently (*i.e.* strongly) with the arachidic acid headgroups to form better ordered CdA Langmuir monolayer, then is it possible to improve the order of the SML structure on the H-terminated surface or to change the unusual growth behavior on the Br-terminated surface? Present study of CdA LB films on differently terminated surfaces using X-ray reflectivity (XRR) and atomic force microscopy (AFM) suggests that better ordered SML structure and normal growth behavior are indeed possible. Regular ring-shaped islands of small heights are also observed, which further suggest the strong role of metal ions and their interaction.

2 Experiment

The preparation of CdA LB films is similar to that of NiA LB films [30]. In brief, arachidic acid ($CH_3(CH_2)_{18}COOH$, Sigma, 99%) molecules were spread from a 0.5 mg/ml chloroform (Aldrich, 99%) solution on Milli-Q water (resistivity 18.2 MΩ cm) containing 0.2 mM cadmium chloride ($CdCl_2.2H_2O$, Merck, 99%) in a Langmuir trough (Apex Instruments). The *p*H of the subphase water was maintained at 8.5–9.0 using sodium hydroxide (NaOH, Merck, 98%) at the time of isotherm measurement (shown in fig. 1) and film deposition. All isotherms and LB depositions were carried out at a speed of 3 mm/min and 2 mm/min, respectively. Film depositions were done in solid phase (shown in fig. 1) at 30 mN/m pressure and at room temperature (22 °C). The deposition pressure was maintained the same as in the case of NiA LB film depositions due to their similar type of isotherm behavior which is evident from fig. 1. The drying time allowed after each upstroke was 10 min at the time of film deposition.

Prior to the deposition, Si substrates were treated differently which lead to differently terminated substrates and were kept inside Milli-Q water. Si substrates were made OH-terminated after keeping them in a mixed solution of ammonium hydroxide (NH_4OH, Merck, 98%), hydrogen peroxide (H_2O_2, Merck) and Milli-Q water ($H_2O : NH_4OH : H_2O_2 = 2 : 1 : 1$, by volume) for 5–10 min at 100 °C. Si substrates were made H-terminated by keeping them in a solution of hydrogen fluoride (HF, Merck, 10%) for 3 min at room temperature (22 °C). Br-terminated Si substrates were made after the removal of the oxide layer by HF etching and keeping them inside the Br-methanol solution (thoroughly rinsed by 0.05% Br-methanol solution). CdA LB films on differently terminated Si substrates were deposited using different numbers of down and/or up strokes of substrates through CdA Langmuir monolayers. On the OH-terminated Si substrate, one CdA LB film was deposited by three strokes (up-down-up) and labeled as 3s-CdA/OH-Si. On the H-passivated Si substrate, one CdA LB film was deposited by two strokes (down-up) and labeled as 2s-CdA/H-Si. Finally on the Br-passivated Si substrate, three CdA LB films were deposited, the first by one stroke (up), the second by two strokes (down-up) and the third by three strokes (up-down-up), labeled as 1s-CdA/Br-Si, 2s-CdA/Br-Si and 3s-CdA/Br-Si, respectively. Films were checked for reproducibility. The transfer ratios for all such LB films depositions were varied from 0.89 to 0.93.

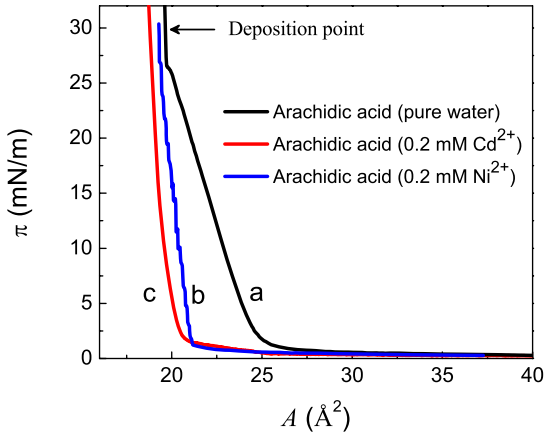

Fig. 1. (Color online) Surface pressure (π)-specific molecular area (A) isotherms at room temperature (22 °C): (a) pure arachidic acid, (b) arachidic acid in the presence of cadmium ions and (c) nickel ions in the subphase water. Compression speed is 3 mm/min for each isotherm. Arrow indicates the point of films deposition by LB method.

XRR measurements [33,34] of the LB films were carried out using a versatile X-ray diffractometer (VXRD) setup. VXRD consists of a diffractometer (D8 Discover, Bruker AXS) with Cu source (sealed tube) followed by a Göbel mirror to select and enhance Cu $K\alpha$ radiation ($\lambda = 1.54$ Å). The diffractometer has a two-circle goniometer (θ-2θ) with quarter-circle Eulerian cradle as sample stage. The latter has two circular (χ and ϕ) and three translational (X, Y, and Z) motions. Scattered beam was detected using NaI scintillation (point) detector. Data were taken in specular condition, *i.e.*, the incident angle (θ) is equal to the reflected angle (θ) and both are in a scattering plane. Under such condition, a nonvanishing wave vector component, q_z, is given by $(4\pi/\lambda)\sin\theta$

with resolution 0.0014 Å^{-1}. XRR data essentially provides electron density profile (EDP), *i.e.* in-plane (x-y) average electron density (ρ) as a function of depth (z) in high resolution [35], from which the structure of the LB film can be obtained [30]. Analysis of X-ray reflectivity data was carried out using Parratt's formalism [36]. In this formalism the reflectivity as a function of q_z for a thin film of finite thickness d over a substrate, is given as $R(q_z) = rr^*$, where

$$r = \frac{r_{12} + r_{23}}{1 + r_{12}r_{23}}, \tag{1}$$

with r_{12} and r_{23} being the reflectance for the vacuum-film and film-substrate interfaces, respectively. The above calculation can be extended for n such thin stratified layers of thickness d and one arrives at a recursive formula in terms of Fresnel reflectance given by

$$r^F_{n-1,n} = \frac{r_{n,n+1} + F_{n-1,n}}{1 + r_{n,n+1}F_{n-1,n}} e^{(-iq_{z,n-1}d_{n-1})}, \tag{2}$$

where

$$F_{n-1,n} = \frac{q_{z,n+1} - q_{z,n}}{q_{z,n+1} + q_{z,n}} \tag{3}$$

In the n-th stratified layer the corresponding wave vector is defined as $q_{z,n} = (q_z^2 - q_{c,n}^2)^{1/2}$. The Fresnel reflectance for the interface between n-th and $(n-1)$-th stratified layer is modified to include the roughness σ_n of the n-th stratified layer and one can finally write the reflectance of a rough surface as

$$r_{n-1,n} = r^F_{n-1,n} e^{\left(-\frac{1}{2}iq_{z,n-1}q_{z,n}\sigma^2\right)}. \tag{4}$$

In general, the electron density variation in a specimen is determined by assuming a model and comparing the simulated profile with the experimental data. EDP is extracted from the fitting of the experimental XRR data. For the fitting each film was divided into a number of layers including roughness as each interface [37]. The chi-square values for XRR data fitting vary from 9.4×10^{-3} to 1.0×10^{-3}.

The topography of the CdA LB films on differently passivated Si(001) substrates was mapped through atomic force microscopy (AFM) technique in different length scales and in different portions, few days after deposition. AFM images were collected in tapping mode to minimize the silicon-tip–induced damage of the soft film. Reproducibility of an image was verified by repeated scans over the same area to exclude any kind of artifacts. WSXM software [38] was used for image processing and analysis.

3 Results and discussion

3.1 Structure and stability of CdA LB films

3.1.1 X-ray reflectivity and electron density profile

XRR data of the 3s-CdA/OH-Si sample collected initially and after 21 days are shown in fig. 2, which are nearly identical. Both data were analyzed considering a thin oxide layer on top of the Si substrate followed by two layers of CdA molecules: AML first and SML on top it. Best-fitted XRR curves thus obtained are shown in fig. 2 and corresponding EDPs are in the inset. EDPs show that the AML/SML structure of the film is near perfect, compact ($\sim$ 95% coverage, considering the electron density of the tail portion (ρ_{tail}) of a perfect and compact structure (either AML or SML) is about 0.32 e Å^{-3}) and stable in ambient condition. Also compared to the film substrate interfacial roughness ($\sigma_{\text{in}} \approx 5$ Å), the top surface roughness of the film ($\sigma_{\text{top}} \approx 3$ Å) is found to be quite small and decreases further (to $\sigma_{\text{top}} \approx 2$ Å) with time. The width of the head portion of the SML structure (d_{H}), obtained from the FWHM of the peak is ~ 8 Å.

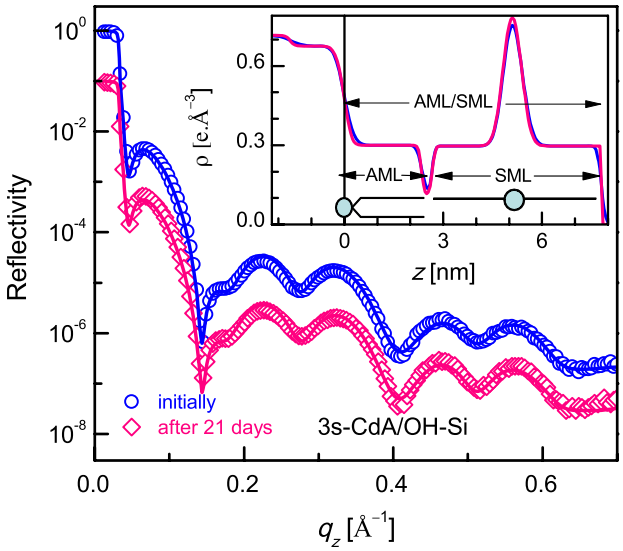

Fig. 2. Time evolution XRR data (different symbols) and analyzed curves (solid line) of CdA LB film on OH-passivated Si substrate, deposited by three strokes. Data and curves are shifted vertically for clarity. Inset: corresponding EDPs showing a possible structure.

XRR data of the 2s-CdA/H-Si sample collected initially and after 33 days are shown in fig. 3. Small changes in the XRR data are observed with time, namely slight smearing of the peak at $q_z \approx 0.3$ Å^{-1} and marginal right shift in the position of the dip at $q_z \approx 0.4$ Å^{-1} and peak at $q_z \approx 0.5$ Å^{-1}. In order to understand the structure of the film and its evolution with time, both reflectivity data were analyzed considering a thin layer on top of the Si substrate followed by SML of CdA molecules. Best-fitted XRR curves thus obtained are shown in fig. 3 and corresponding EDPs are in the inset. It is clear from the EDPs that the structure of the film remains almost unchanged with time. What is changed is the film-substrate interfacial region, namely the decrease of electron density due to the formation of oxides at the Si surface. Interestingly, such change in the interface cannot disturb the quite perfect and compact ($\sim$ 80% coverage) SML structure of the film. The top surface roughness of the film ($\sigma_{\text{top}} \approx$ 4 Å) is found quite small compared to the film-substrate

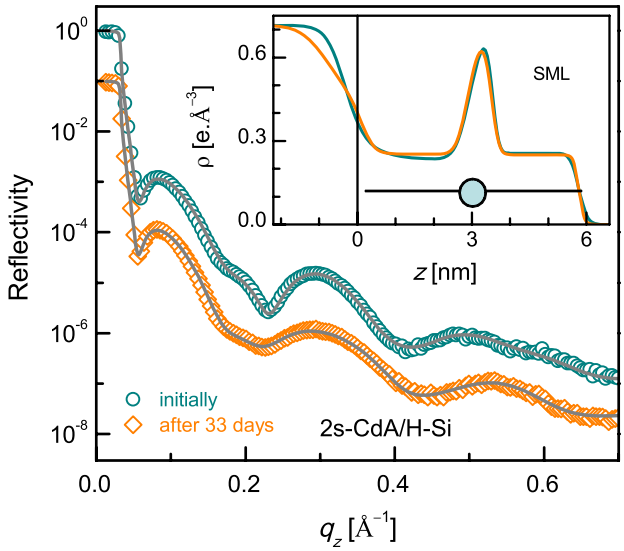

Fig. 3. (Color online) Time evolution XRR data (different symbols) and analyzed curves (solid line) of CdA LB film on H-passivated Si substrate, deposited by two strokes. Data and curves are shifted vertically for clarity. Inset: corresponding EDPs showing a possible structure.

interfacial roughness ($\sigma_{\rm in} \approx 8$ Å), indicating the tendency of CdA molecules to form an ordered SML structure. This tendency continues with time and improves the ordering even after the formation of oxides at the interface, which is evident from the further decrease of the top surface roughness (to $\sigma_{\rm top} \approx 3$ Å). The value of $d_{\rm H}$ is ~ 8 Å, which means that the ordering of the head-groups of this film is comparable to that of the 3s-CdA/OH-Si sample.

XRR data and analyzed curves of 1s-CdA/Br-Si, 2s-CdA/Br-Si and 3s-CdA/Br-Si samples are shown in fig. 4. EDPs obtained from the analysis of XRR data are included in the insets of fig. 4. EDP suggests that the AML structure with reduced thickness is formed on Br-terminated Si surface by single up stroke of deposition. The reduced thickness probably indicates the imperfect nature of the film. In the XRR data of 2s-CdA/Br-Si and 3s-CdA/Br-Si samples, a small hump near $q_z = 0.18$ Å^{-1} is observed initially, which vanishes with time. However, from the EDPs not much change is observed in the films with time. The structure of the 2s-CdA/Br-Si sample is AML+SML, *i.e.* both AML (of height ≈ 2.2 nm) and SML (of height ≈ 4.2 nm) structures are present on the substrate surface side by side (in-plane). The reduced thickness observed for both kinds of layers is related to their imperfect nature. The amount of SML molecules is relatively small compared to AML molecules. The amount of the latter seems to be comparable to that in the 1s-CdA/Br-Si sample. Due to the imperfect nature of the film, some heads are always contributing in the electron density of the tail portion. Considering $\rho_{\rm tail} \approx 0.4$ e Å^{-3} for full coverage with imperfect structure, the coverage of 1s-CdA/Br-Si sample with AML structure is about 75%. The coverage of 2s-CdA/Br-Si sample with AML structure is again 75%, which increases marginally with time

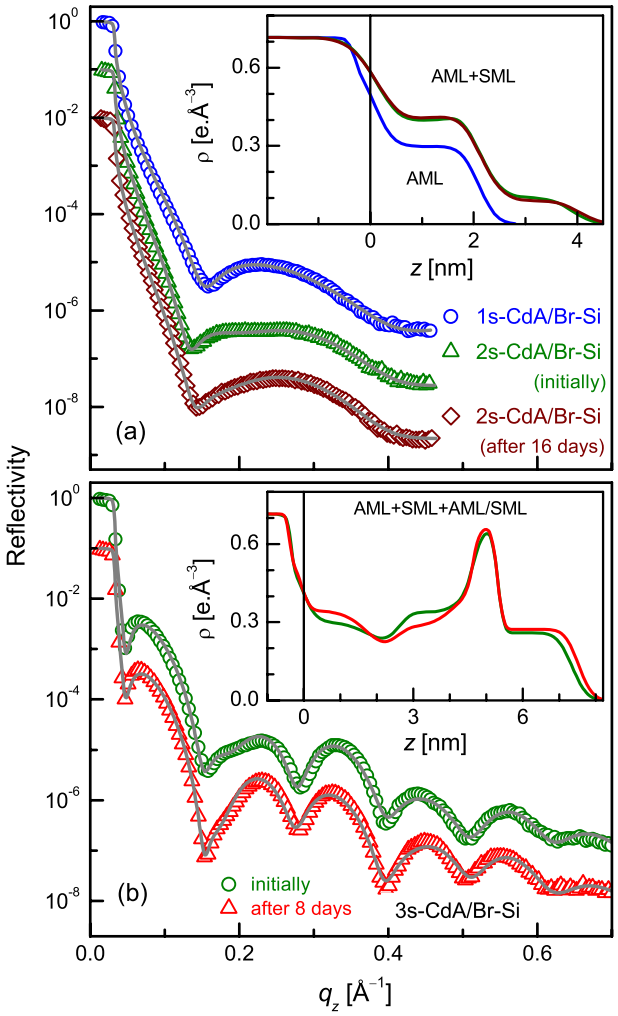

Fig. 4. (Color online) Time evolution XRR data (different symbols) and analyzed curves (solid line) of CdA LB films on Br-passivated Si substrates, deposited by (a) one and two strokes and (b) three strokes. In each panel, data and curves are shifted vertically for clarity. Inset: corresponding EDPs, indicating possible structures.

and the rest with SML structure decreases accordingly. This indicates that the imperfect structures are quite stable.

EDPs of the 3s-CdA/Br-Si sample (inset of fig. 4) are slightly different from those of 3s-CdA/OH-Si sample (inset of fig. 2), which indicates the presence of some other structures apart from the AML/SML structure. To find out all the structures along with the individual contributions (roughly), EDPs of the 3s-CdA/Br-Si sample were deconvoluted which is shown in fig. 5. It is found that initially the film consists of mainly two different structures: AML/SML and SML, of which AML/SML is the majority. In SML structure not all molecules lie in same vertical position, some are attached directly to the substrate (labeled as B1 type) and others are slightly shifted upwards (labeled as B2 type). Shifting of SML (B2 type) in the upward direction does not necessarily take place to a particular height, rather it is reasonable to consider a distri-

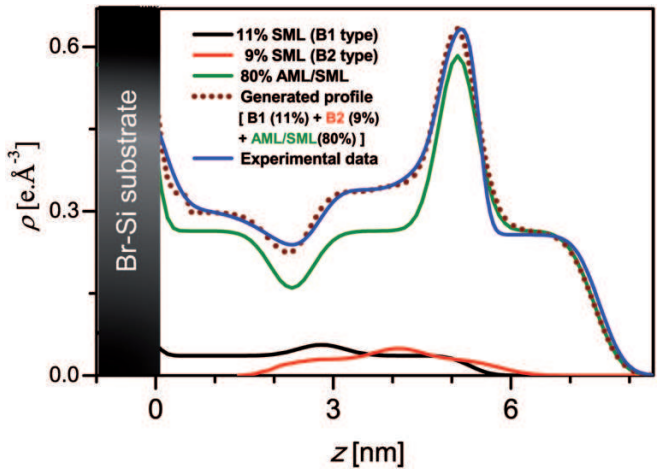

Fig. 5. (Color online) Deconvolution of EDP of 3s-CdA/Br-Si sample suggests that the film consists of three different structures, *i.e.*, $\sim$ 11% SML (B1 type), $\sim$ 9% SML (B2 type) and $\sim$ 80% AML/SML. Adding these structures a EDP is generated which is very similar to the experimental EDP.

bution in shifting which reveals itself as a broadening of the head part with a low ρ value (fig. 5). Initially no AML structure is observed in fig. 5, but finally after reorganization with time few AML structured molecules are observed along with other structures (not shown here). The increment of the ρ value of the lower tail part of thickness 2 nm indicative of the formation of the AML structure. However, the deconvoluted EDP (fig. 5) indicates that the LB film initially consists of $\sim$ 11% SML (B1 type), $\sim$ 9% SML (B2 type) and $\sim$ 80% AML/SML structures. Finally few SML structured molecules (both B1 and B2 types) flip to form the AML structure whose coverage is found to observe $\sim$ 10%. The coverage of AML/SML structure remains nearly the same around 80%. Thus the deconvolution of EDP clearly monitors the changes happening in the film quantitatively. Still, there may be some errors in estimating the coverage of individual structures as those are not perfect structures.

3.1.2 Atomic force microscopy and topography

Typical AFM images of CdA LB films deposited on differently treated Si(001) substrates are shown in fig. 6. The corresponding model structures are also shown in fig. 6. The AFM image of 3s-CdA/OH-Si sample (fig. 6(a)) shows that it consists of pinhole-type defects, which are large in number but small in size. Otherwise the surface is very smooth. The maximum depth of the defects is about 8 nm, which corresponds to the Si surface relative to the AML/SML structured smooth film. Considering the XRR results, pinhole-like defects cover about 5% of the surface. Figure 6(d) schematically shows the structure of the film. AFM image of 2s-CdA/H-Si sample (fig. 6(b)) shows that the top surface of the film is quite smooth, which is consistent with the XRR results. However, AFM images collected in larger length scale (not shown here) indicate

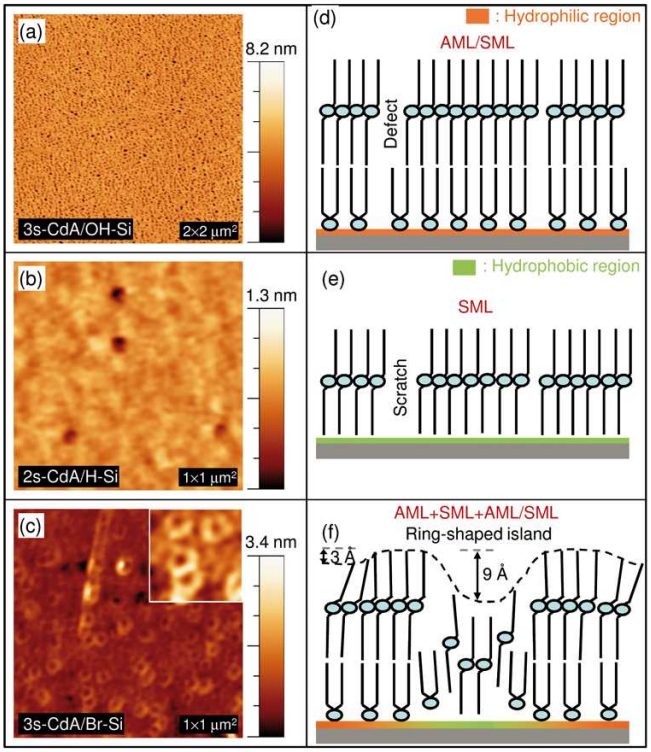

Fig. 6. (Color online) AFM images showing the topography of CdA LB films (a) on OH-terminated Si substrate, deposited by three strokes, of scan size $2\times2\,\mu m^2$, (b) on H-passivated Si(001) substrate, deposited by two strokes, of scan size $1\times1\,\mu m^2$ and (c) on Br-terminated Si substrate, deposited by three strokes, of scan size $1\times1\,\mu m^2$. Inset: magnified image of scan size $200\times200\,nm^2$. (d)-(f) Model structures of the films corresponding to the AFM images (a)-(c).

the presence of some line-strip–like scratches in smooth film. Although the origin of such scratches is not clear, their presence probably lowers the coverage of the film to $\sim$ 80%, as predicted by EDP. Also, such scratches help to estimate the film thickness, and hence the structure of the film, which is SML as shown schematically in fig. 6(e). The AFM image of the 3s-CdA/Br-Si sample (fig. 6(a)) is quite interesting. It shows the presence of ring-shaped islands having size of about 70 nm and an annular width about 25 nm. However, the ring-shaped islands do not lie on a flat surface, which is clear from the magnified view as shown in the inset, rather the depth inside ($\sim$ 9 Å) is higher compared to the depth outside ($\sim$ 3 Å). Considering the XRR results, the structures corresponding to the inside and outside portions of the ring-shaped island are SML and AML/SML, respectively. The structure of the island itself is also AML/SML, but such structure is probably more compact and ordered compared to that of the outside portion, which gives rise to a small height difference. This is shown schematically in fig. 6(f). It is necessary to mention that no such ring-shaped islands are present in 1s-CdA/Br-Si and 2s-CdA/Br-Si samples.

In order to find out the role of Br concentration in such a type of pattern formation we also prepared another two

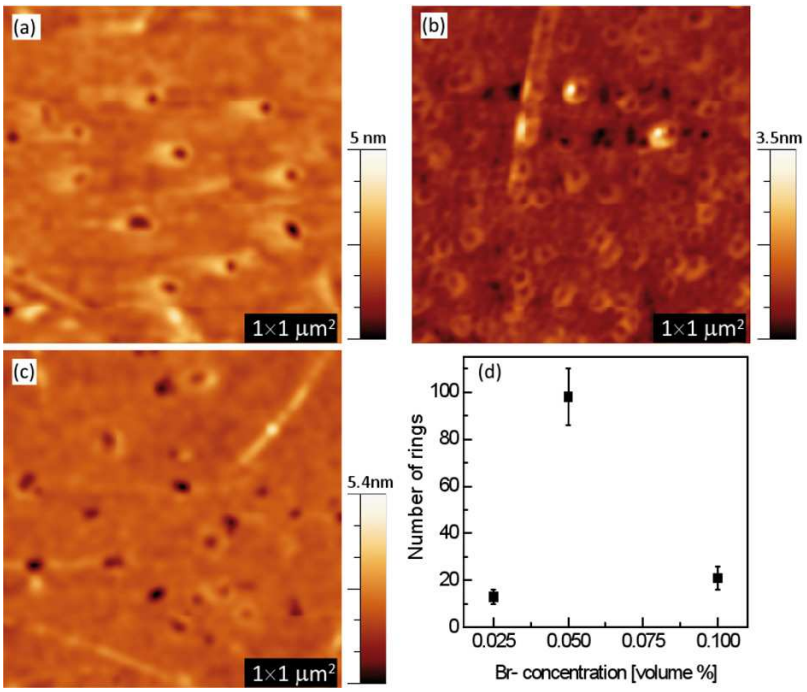

Fig. 7. (Color online) AFM images showing the topography of CdA LB films on Br-passivated substrates prepared in three different concentrations of Br: (a) 0.025%, (b) 0.05% and (c) 0.1% by volume in Br-methanol solution. (d) Number of rings (per μm^2 area) for the three different concentrations of Br.

Table 1. Different layered structures for CdA and NiA LB films on differently passivated Si substrates deposited by different number (n) of strokes and relevant parameters such as film-substrate interfacial roughness (σ_{in}), top surface roughness of the film (σ_{top}), and head width (d_H) corresponding to the SML structure obtained from the analysis of XRR data and AFM images.

		OH-Si				H-Si				Br-Si
LB film	n	Structure	σ_{in} (Å)	σ_{top} (Å)	d_H (Å)	Structure	σ_{in} (Å)	σ_{top} (Å)	d_H (Å)	Structure
CdA	1	AML				–				AML
	2	–				SML	8–12	4–3	8	AML+SML
	3	AML/SML	5	3–2	8	–				AML+SML+AML/SML
NiA	1	AML				–				AML+SML
	2	–				SML	6–10	9–14	11	AML+SML
	3	AML/SML	6	7	10	–				AML+SML+AML/SML+SML/SML

LB films in three strokes by using two different Br concentrations, which are $\sim 0.1\%$ and 0.025% by volume, for Br-passivation. The AFM images of these two films along with the previous sample ($\sim 0.05\%$ Br concentration) are given in fig. 7. The same ring-shaped nanopattern is observed, but there is a drastic difference in the number of ring-shaped islands as shown in fig. 7(d). In comparison with the medium concentration of Br (0.05%), very few ring-shaped islands were observed in higher (0.1%) and lower (0.025%) Br-concentrated sample.

3.2 Structure formation mechanism of LB films

In order to understand the mechanism behind the formation of different structures of CdA LB films on differently passivated Si surfaces, let us first compare the structures of the present films with those of the NiA LB films studied earlier [30]. Table 1 summarizes different structures present in CdA and NiA films on three differently passivated Si surfaces deposited in different number of strokes. Also different parameters, such as film-substrate interfacial roughness (σ_{in}), top surface roughness of the film (σ_{top}) and head width corresponding to the SML structure (d_H) for LB films on OH-Si and H-Si substrates are included in table 1, which will be important in understanding the differences in the structures. Similar to the CdA films, the values of these parameters for the NiA LB films are estimated from the EDPs in ref. [30].

On OH-terminated Si substrates, both CdA and NiA LB films form an AML structure in single up stroke of

deposition and an AML/SML structure in three strokes of deposition, which are consistent with the hydrophilic nature of the OH-terminated Si substrate. Film coverage ($\sim$ 95%) and film-substrate interfacial roughness of the 3s-CdA/OH-Si sample are found similar to those of the 3s-NiA/OH-Si sample, indicating that these two parameters are film- (*i.e.* head-groups) independent and mainly related to the nature of the substrate. The values of $\sigma_{\rm top}$ and $d_{\rm H}$ for the 3s-CdA/OH-Si sample are found smaller compared to those for the 3s-NiA/OH-Si sample, suggesting better ordering of the Cd head-groups compared to the Ni head-groups. With time, such ordering either remains the same (for the NiA LB film) or even improves (for the CdA LB film). The latter is evident from the decrease (whatever small) in the value of $\sigma_{\rm top}$ (from 3 Å to 2 Å) with time.

The CdA LB film forms an SML structure on H-terminated Si substrate in two strokes of deposition similar to the NiA LB film, which is well understood from the hydrophobic nature of the H-terminated Si substrate. Comparison of different parameters, namely $\sigma_{\rm top}$ and $d_{\rm H}$ for the two films suggests that the ordering of the Cd head-groups is better compared to the Ni head-groups, while the AFM images and the EDPs suggest that the structure of the CdA LB film is more compact. However with time, oxides grow on the Si substrate, which increases the film-substrate interfacial roughness. Oxide growth destabilizes and deteriorates the structure of the NiA film, which is evident from the increase in the value of $\sigma_{\rm top}$ (from 9 Å to 14 Å) with time. However, unlike NiA film, oxide growth does not deteriorate the structure of the CdA film, rather improves the ordering, which is evident from the decrease (whatever small) in the value of $\sigma_{\rm top}$ (from 4 Å to 3 Å) with time.

CdA and NiA LB films on Br-terminated Si substrate deposited by two (down-up) strokes, show similar (AML+SML) structure. This is consistent with the coexisting (hydrophilic-hydrophobic) nature of the Br-terminated Si surface, where the SML structure is formed on the hydrophobic portion during down-up stroke and the AML structure is formed on the hydrophilic portion during up stroke only. Due to the inhomogeneous and unstable nature of the Br-terminated Si surface, it is expected that prior to the deposition, oxide layer might have grown in some portion of the surface replacing the Br atoms [30]. Large coverage of AML structure compared to SML structure suggests that the Br-terminated Si surface is mostly ($\sim$ 75%) composed of hydrophilic portion and remains unchanged, while the imperfect nature of both AML and SML structures indicates that the hydrophilicity and hydrophobicity of the respective portions of such Si surface are weak.

Structures of CdA LB films on Br-terminated Si substrates deposited by an odd number of strokes are quite different from those of NiA LB films. In single up stroke of deposition, the CdA LB film forms an AML structure with partial coverage, while both AML and SML structures are observed for the NiA LB film. Due to the coexisting (hydrophilic-hydrophobic) nature of the Br-terminated Si surface, growth of AML structure on the hydrophilic portion of the substrate in single up stroke of deposition is quite natural, which is the case for the CdA LB film. Also this suggests that during up stroke of deposition, continuous diffusion and configurational change (or flipping) of molecules from hydrophilic to nearly hydrophobic portion, which was proposed for the unusual AML+SML structure of the NiA LB film [30], do not take place in case of CdA molecules.

In three stokes of deposition, a CdA LB film forms an AML+SML+AML/SML structure on Br-terminated Si substrate, unlike NiA LB film, which forms AML+SML+AML/SML+SML/SML structure. The formation of the structure for the NiA LB film has been understood considering further growth on AML+SML structured LB film having stress across the hydrophobic/hydrophilic interface (that developed in one stroke of deposition), by down-up stroke of deposition [30]. Release of stress also takes place in subsequent down-up stroke of deposition, which allows some molecules to flip off from the substrate and dump across the hydrophobic/hydrophilic interface to form large-heights ring-shaped islands. On the other hand, the SML+AML/SML structure, with AML/SML as majority ($\sim$ 80%) is expected for CdA LB film. In fact, that is what we observed initially, with slight modification, namely all molecules of the SML structure do not lie in the same vertical plane. Molecules close to the hydrophobic/hydrophilic interface detach from the substrate and shift upwards (B2 type) with respect to the rest (B1 type). Probably, oxide growth at the initial stages has a weak hydrophilicity and can only shift SML structured molecules slightly upwards, but cannot change the configuration of the molecules. With time, hydrophilicity increases and a change in the configuration of molecules (from SML to AML) takes place, which creates in-plane pressure. This pressure is mostly exerted on the AML/SML structured molecules close to the hydrophobic/hydrophilic interface making the molecules compact and straight compared to the rest and showed up as small-heights ring-shaped islands. It can be noted that unlike NiA LB film, dumping of molecules across the hydrophobic/hydrophilic interface, by flipping up from the substrate to release the stress, never occurs in the CdA LB film. A number of such ring-shaped islands strongly depends upon the number of hydrophilic/hydrophobic domains, which becomes maximum at 0.05% Br concentration, as this concentration may be the most favorable for Br-passivation [39].

It is clear from the observed structures that the LB films with Cd head-groups are more ordered compared to those with Ni head-groups although they have deposited in the same solid phase condition (fig. 1). This can be understood considering the interaction (E) between the head-groups [40] and the bond strength (D) between the metal ion and carboxylic ligand (CL) [32]. The interaction between the head-groups becomes stronger in the presence of Cd ions rather than Ni ions (*i.e.* $E_{\rm Cd\text{-}Cd} > E_{\rm Ni\text{-}Ni}$). A strong interaction between Cd head-groups holds the adjacent molecules rigidly and makes them ordered. Also the metal ion-ligand bond strength is stronger in the case of Cd ion compared to Ni ion (*i.e.* $D_{\rm Cd\text{-}CL} > D_{\rm Ni\text{-}CL}$) [32].

Such bond strength difference is found to influence the patterns of the amphiphilic molecules, which lie horizontally on the HOPG substrate in the head-to-head and tail-to-tail configuration [32]. Metal ion specific bonding effect is also observed in the structure of the vertically aligned Langmuir monolayers or films [3, 5]. The difference between the structures of CdA and NiA LB films observed here clearly suggests that the bond strength for the CdA molecules is better compared to that for the NiA molecules. Accordingly (considering both head-head interaction and metal ion-carboxylic ligand bond strength), CdA molecules are well ordered, coupled and cannot flip easily, while NiA molecules are relatively flexible and can flip. The growth of the LB films depends on the status of the passivated Si surfaces at the time of LB deposition and its stability depends on the further reactivity of the Si surface with the environmental oxygen. It is reported that if free metal ions are present on the Si surface, they can weaken the Si-Si bond in order to react with the Si [41–44]. Even metal bearing head-group of amphiphilic molecules can react with the underlying substrate as we have observed in our previous study on Ni ion [45]. Such reaction of LB films with the passivated Si surface was not observed in the case of Cd ion-bearing head-group [46]. The evolution of the grown CdA LB films on the passivated Si surfaces with time is mainly related with the long-term reactivity of the passivated Si with the atmospheric oxygen which is the most favorable reaction as they form highly stable silicon oxide compounds. No such enhanced oxidation of passivated Si surfaces after the attachment of the CdA LB films was observed [46]. A probable reason is the strong covalent bonding between Cd ion and ligand which does not allow to disrupt the bonding between passivating element and the Si atom.

4 Conclusions

Structure and stability of CdA LB films on homogeneously and heterogeneously passivated Si surfaces were studied using XRR and AFM techniques and compared with those of NiA LB films. Hydrophilic, hydrophobic and coexisting natures of the OH-, H- and Br-passivated Si surfaces, respectively, are clearly evident from the structures of the CdA LB films, similar to those observed from the NiA LB system. The order of the Cd head-groups in the SML structure, formed directly on the hydrophobic Si surface or through the AML structure on the hydrophilic Si surface, is found to be far better compared to that of the Ni head-groups. This clearly suggests that $E_{\text{Cd-Cd}} > E_{\text{Ni-Ni}}$, *i.e.* the interaction between Cd head-groups is stronger compared to that between Ni head-groups and/or $D_{\text{Cd-CL}} > D_{\text{Ni-CL}}$, *i.e.* the bond strength between the Cd ion and the carboxylic ligand is better compared to that between the Ni ion and the carboxylic ligand. The influence of such effects is also observed for the LB films on the Br-terminated Si surface. For example, CdA molecules show that they are coupled and cannot flip easily, while NiA molecules show that they are flexible and can flip easily either from hydrophilic to nearby hydrophobic portion of the Si surface during a single stroke of deposition or from the substrate and dumping of molecules across the hydrophobic/hydrophilic interface to release the stress in the structure of the film during three strokes of deposition. Ring-shaped islands are also observed in the CdA LB film, across the hydrophobic/hydrophilic interface, which are quite regular but small in heights and the effect is more like buckling, rather than collapse.

References

1. A. Ulman, *Introduction to Ultrathin Organic Films* (Academic Press, New York, 1991).
2. D.K. Schwartz, Surf. Sci. Rep. **27**, 245 (1997).
3. V.M. Kaganer, H. Möhwald, P. Dutta, Rev. Mod. Phys. **71**, 779 (1999).
4. F. Leveiller, D. Jacquemain, M. Lahav, L. Leiserowitz, M. Deutsch, K. Kjaer, J. Als-Nielsen, Science **252**, 1532 (1991).
5. J. Kmetko, A. Datta, G. Evmenenko, P. Dutta, J. Phys. Chem. B **108**, 10818 (2001).
6. V. Dupres, S. Cantin, F. Benhabib, F. Perrot, P. Fontaine, M. Goldmann, J. Daillant, O. Konovalov, Langmuir **19**, 10808 (2003).
7. K.B. Blodgett, I. Langmuir, Phys. Rev. **51**, 964 (1937).
8. M.C. Petty, *Langmuir-Blodgett Films: An Introduction* (Cambridge University Press, New York, 1996).
9. I.R. Peterson, J. Phys. D **23**, 379 (1990).
10. C.P. Collier, R.J. Saykally, J.J. Shiang, S.E. Henrichs, J.R. Heath, Science **277**, 1978 (1997).
11. K. Tollner, R. Popovitz-Biro, M. Lahav, D. Milstein, Science **278**, 2100 (1997).
12. R. Singhal, A. Chaubey, K. Kaneto, W. Takashima, B.D. Malhotra, Biotechnol. Bioeng. **85**, 277 (2004).
13. K. Hosoki, T. Tayagaki, S. Yamamoto, K. Matsuda, Y. Kanemitsu, Phys. Rev. Lett. **100**, 207404 (2008).
14. D.K. Schwartz, J. Garnaes, R. Viswanathan, S. Chiruvolu, J.A. Zasadzinski, Phys. Rev. E **47**, 1267 (1993).
15. J.B. Peng, G.T. Barnes, I.R. Gentle, G.J. Foran, J. Phys. Chem. B **104**, 5553 (2000).
16. S. Kundu, A. Datta, S. Hazra, Chem. Phys. Lett. **405**, 282 (2005).
17. S. Milner, J.F. Joanny, P. Pincus, Europhys. Lett. **9**, 495 (1989).
18. M.M. Lipp, K.Y.C. Lee, D.Y. Takamoto, J.A. Zasadzinski, A.J. Waring, Phys. Rev. Lett. **81**, 1650 (1998).
19. C. Fradin, A. Braslau, D. Luzet, M. Alba, C. Gourier, J. Daillant, G. Grübel, G. Vignaud, J.F. Legrand, J. Lal, J.M. Petit, F. Rieutord, Physica B **248**, 310 (1998).
20. H.E. Ries jr., Nature **281**, 287 (1979).
21. C. Ybert, W. Lu, G. Möller, C.M. Knobler, J. Phys. Chem. B **106**, 2004 (2002).
22. S. Kundu, A. Datta, S. Hazra, Phys. Rev. E **73**, 051608 (2006).
23. D. Vaknin, W. Bu, S.K. Satija, A. Travesset, Langmuir **23**, 1888 (2007).
24. K.Y.C. Lee, Annu. Rev. Phys. Chem. **59**, 771 (2008).
25. B. Kumar, K.A. Suresh, S.K. Gupta, S. Kumar, J. Chem. Phys. **133**, 044701 (2010).
26. H.F. Okorn-Schmidt, IBM J. Res. Develop. **43**, 351 (1999).
27. X.G. Zhang, *Electrochemistry of Silicon and Its Oxide* (Kluwer Academic Publishers, New York, 2004).

28. C.-Y. Ruan, V.A. Lobastov, F. Vigliotti, S. Chen, A.H. Zewail, Science **304**, 80 (2004).
29. J.K. Bal, S. Hazra, Phys. Rev. B **79**, 155412 (2009).
30. J.K. Bal, S. Kundu, S. Hazra, Phys. Rev. B **81**, 045404 (2010).
31. P.L. Silvestrelli, F. Toigo, F. Ancilotto, J. Phys. Chem. B **110**, 12022 (2006).
32. W. Dong, R. Wang, G. Mao, H. Möhwald, Soft Matter **2**, 686 (2006).
33. I.K. Robinson, D.J. Tweet, Rep. Prog. Phys. **55**, 599 (1992).
34. J. Daillant, A. Gibaud (Editors), *X-ray and Neutron Reflectivity: Principles and Applications* (Springer, Paris, 1999).
35. J.K. Bal, S. Hazra, Phys. Rev. B **75**, 205411 (2007).
36. L.G. Parratt, Phys. Rev. **95**, 359 (1954).
37. S. Kundu, S. Hazra, S. Banerjee, M.K. Sanyal, S.K. Mandal, S. Chaudhuri, A.K. Pal, J. Phys. D **34**, L73 (1998).
38. I. Horcas, R. Fernndez, J.M. Gwez-Rodrguez, J. Colchero, J. Gomez-Herrero, A.M. Baro, Rev. Sci. Instrum. **78**, 013705 (2007).
39. M.J. Bedzyk, W. Gibson, J.A. Golovchenko, J. Vac. Sci. Technol. **20**, 634 (1982).
40. D.K. Schwartz, J. Garnaes, R. Viswanathan, J.A. Zasadzinski, Science **257**, 508 (1992).
41. T. Hanada, M. Kawai, Vacuum **41**, 650 (1990).
42. D. Graf, M. Grundner, D. Muhlhoff, M. Dellith, J. Appl. Phys. **69**, 7620 (1991).
43. S. Xu, P. Xu, M. Ji, X. Liu, M. Ma, J. Zhu, Y. Zhang, J. Mater. Sci. Technol. **9**, 437 (1993).
44. N. Takano, N. Hosoda, T. Yamada, T. Osaka, Electrochim. Acta **44**, 3743 (1999).
45. J.K. Bal, S. Kundu, S. Hazra, Chem. Phys. Lett. **500**, 90 (2010).
46. J.K. Bal, S. Kundu, S. Hazra, Mater. Chem. Phys. **134**, 549 (2012).